J Sci Comput (2017) 71:414–434
DOI 10.1007/s10915-016-0305-7

A High Order Multi-Dimensional Characteristic Tracing Strategy for the Vlasov–Poisson System

Jing-Mei Qiu[1] · **Giovanni Russo**[2]

Received: 11 December 2015 / Revised: 27 July 2016 / Accepted: 6 October 2016 /
Published online: 28 October 2016

Abstract In this paper, we consider a finite difference grid-based semi-Lagrangian approach for solving the Vlasov–Poisson (VP) system. Many of existing methods are based on dimensional splitting, which decouples the problem into solving linear advection problems, see Cheng and Knorr (J Comput Phys 22:330–351, 1976). However, such splitting is subject to the splitting error. If we consider multi-dimensional problems without splitting, difficulty arises in tracing characteristics with high order accuracy. Specifically, the evolution of characteristics is subject to the electric field which is determined globally from the distribution of particle density via Poisson's equation. In this paper, we propose a novel strategy of tracing characteristics high order in time via a two-stage multi-derivative prediction–correction approach and by using moment equations of the VP system. With the foot of characteristics being accurately located, we propose to use weighted essentially non-oscillatory interpolation to recover function values between grid points, therefore to update the solution at the next time level. The proposed method does not have time step restriction as the Eulerian approach and enjoys high order spatial and temporal accuracy. The performance of the proposed schemes are numerically demonstrated via classical test problems such as Landau damping and two stream instabilities.

Keywords Semi-Lagrangian · Vlasov–Poisson system · Characteristics · High order · WENO

Jing-Mei Qiu: Research supported by Air Force Office of Scientific Computing YIP Grant FA9550-12-0318, NSF Grant DMS-1217008 and DMS-1522777.
Giovanni Russo: Research supported by ITN-ETN Marie Curie Program 642768.

✉ Jing-Mei Qiu
jingqiu@math.uh.edu

Giovanni Russo
russo@dmi.unict.it

[1] Department of Mathematics, University of Houston, Houston, TX 77004, USA

[2] Department of Mathematics and Informatics, University of Catania, 95125 Catania, Italy

1 Introduction

This paper focuses on a high order truly multi-dimensional semi-Lagrangian (SL) approach for the Vlasov–Poisson (VP) simulations. Arising from collisionless plasma applications, the VP system,

$$\frac{\partial f}{\partial t} + \mathbf{v} \cdot \nabla_{\mathbf{x}} f + \mathbf{E}(\mathbf{x}, t) \cdot \nabla_{\mathbf{v}} f = 0, \tag{1.1}$$

and

$$\mathbf{E}(\mathbf{x}, t) = -\nabla_{\mathbf{x}} \phi(\mathbf{x}, t), \quad -\Delta_{\mathbf{x}} \phi(\mathbf{x}, t) = \rho(\mathbf{x}, t) - 1, \tag{1.2}$$

describes the temporal evolution of the particle distribution function in six dimensional phase space. $f(\mathbf{x}, \mathbf{v}, t)$ is probability distribution function which describes the probability of finding a particle with velocity $\mathbf{v}$ at position $\mathbf{x}$ at time t, $\mathbf{E}$ is the electric field, and ϕ is the self-consistent electrostatic potential. The probability distribution function couples to the long range fields via the charge density, $\rho(t, x) = \int_{\mathbb{R}^3} f(x, v, t) dv$, where we take the limit of uniformly distributed infinitely massive ions in the background. In this paper, we consider the VP system with 1-D in $\mathbf{x}$ and 1-D in $\mathbf{v}$.

Many different approaches have been proposed for the VP simulations. There are the Lagrangian particle-in-cell (PIC) methods, which have been very popular in practical high dimensional simulations due to their relatively low computational cost [22,26,28]. However, the Lagrangian particle approach is known to suffer from statistical noise which is of order $1/\sqrt{N}$, where N is the number of particles in a simulation. There are very high order Eulerian finite difference [37], finite volume [1], finite element discontinuous Galerkin methods [10,25]. Eulerian methods can be designed to be highly accurate in both space and in time, thus being able to resolve complicated solution structures in a more efficient manner by using a set of relatively coarse numerical mesh. However, they are subject to CFL time step restrictions. There are the dimensional split SL approach originally proposed in [8], and further developed in the finite volume [2,3,16,20,34], finite difference [5,30,31], finite element discontinuous Galerkin framework [32,33] and a hybrid finite different-finite element framework [24]. The semi-Lagrangian framework allows for extra large numerical time steps compared with Eulerian approach, leading to some savings in computational cost. The dimensional splitting allows for a very simple implementation procedure for tracing characteristics; classical Strang-splitting is second order accurate, however it causes an operator splitting error in time, which for example, prevents the construction of well balance schemes that maintain the stationary solution. For convergence estimate for the semi-Lagrangian methods for the VP simulations, we refer to [7]. If the splitting is not performed properly, numerically instabilities are observed [27]. In [6,9,23], high order dimensional splitting techniques have been applied to the VP simulations. In [11], an integral deferred correction method is proposed for the dimensional split SL approach to reduce the splitting error in VP simulations. There have been unsplit semi-Lagrangian solvers [12,18]. However, high order ways of tracing characteristics for the nonlinear VP system is still lacking.

In this paper, we propose a high order truly multi-dimensional SL finite difference approach for solving the VP system. The 'truly multi-dimensional' means that no operator splitting is involved. The difficulty is the tracing of characteristics with high order temporal accuracy in a time step. Especially the evolution of characteristics is due to the electric field induced by the unknown particle distribution function f in the Vlasov Eq. (1.1). A high order two-stage multi-derivative predictor–corrector algorithm is proposed to build up a high order characteristic-tracing algorithm based on lower order ones, with the help of moment equations of the VP system. A high order WENO interpolation is proposed to recover information

among grid points. The proposed algorithm is of high order accuracy in both phase space and in time. We also discuss the computational cost of the proposed algorithm. Finally, we remark that there is no mass conservation, resolving which is the topic for our future investigation.

The paper is organized as follows. Section 2 describes the high order SL finite difference approach without operator splitting. High order way of tracing characteristics are proposed and analyzed. Issues related to computational cost are discussed. Section 3 presents numerical simulation results. Finally, the conclusion is given in Sect. 4.

2 Truly Multi-Dimensional SL Algorithm

2.1 Algorithm Framework

Our goal is to design a high order SL finite difference scheme for the VP system without operator splitting. Consider the VP system (1.1) with 1-D in x and 1-D v. The 2-D $x-v$ plane is discretized into uniformly spaces rectangular meshes,

$$\begin{aligned} x_{\frac{1}{2}} < x_{1+\frac{1}{2}} < \cdots < x_{i+\frac{1}{2}} < \cdots < x_{n_x+\frac{1}{2}}, \\ v_{\frac{1}{2}} < v_{1+\frac{1}{2}} < \cdots < v_{j+\frac{1}{2}} < \cdots < v_{n_v+\frac{1}{2}}. \end{aligned}$$

The center of each of the rectangular cell $[x_{i-\frac{1}{2}}, x_{i+\frac{1}{2}}] \times [v_{j-\frac{1}{2}}, v_{j+\frac{1}{2}}]$ is denoted as (x_i, v_j). We consider evolving the numerical solution $f^n_{i,j}$, $i = 1, \cdots n_x$, $j = 1, \cdots, n_v$, where $f^n_{i,j}$ denotes the numerical solution at (x_i, v_j) at the time level t^n. The proposed SL algorithm in updating the solution f^{n+1}_{ij} consists of the following steps.

1. Characteristics are traced backward in time to t^n. Let the foot of the characteristic at the time level t^n emanating from (x_i, v_j) at t^{n+1} be denoted as $(x^\star_i, v^\star_j)$. It is approximated by numerically solving the following final value problem

$$\begin{cases} \frac{dx(t)}{dt} = v(t), \\ \frac{dv(t)}{dt} = E(x(t), t), \\ x(t^{n+1}) = x_i, \\ v(t^{n+1}) = v_j. \end{cases} \tag{2.1}$$

   Here, we remark that solving (2.1) with high order temporal accuracy is non-trivial. Especially, the electric field E depends on the unknown function f via Poisson's Eq. (1.2) in a global rather than local fashion. Moreover, being a final value problem, the electric field E is known initially only at the time step t^n. In Sect. 2.2, we discuss the proposed high order (up to third order) way of tracing characteristics in time.
2. The solution is updated as

$$f^{n+1}_{i,j} = f(x^{n,(l)}_i, v^{n,(l)}_j, t^n) \approx f(x^\star_i, v^\star_j, t^n). \tag{2.2}$$

   We propose to recover $f(x^{n,(l)}_i, v^{n,(l)}_j, t^n)$ by a high order (up to sixth order) WENO interpolation from $f^n_{i,j}$, $i = 1, \cdots n_x$, $j = 1, \cdots, n_v$. Here the superscript (l) denotes the formal order of temporal approximation in locating the feet of characteristics. The procedures are discussed in Sect. 2.3.

2.2 Tracing Characteristics with High Order Temporal Accuracy

It is numerically challenging to design a one-step method to locate the foot of characteristics with high order accuracy in time. The electric field E is not explicitly unknown; it is induced by the unknown function f via the Poisson's Eq. (1.2). Since it is difficult to evaluate the electric field E [r.h.s. of Eq. (2.1)] for some intermediate time stages between $[t^n, t^{n+1}]$, Runge–Kutta methods can't be used directly.

Below we describe our proposed predictor-corrector procedure for locating the foot of characteristics. We will first describe a first order scheme in tracing characteristics; the second scheme is built upon the first order prediction; and the proposed third order scheme is built upon the second order prediction. In our notations, the superscript ^{n} denotes the time level, the subscript i and j denote the location x_i and v_j in x and v directions respectively, the superscript $^{(l)}$ denotes the formal order of approximation. For example, in Eq. (2.3) below, $x_i^{n,(1)}$ (or $v_j^{n,(1)}$) approximates $x_i^\star$ (or $v_j^\star$) with first order, and $E_i^n = E(x_i, t^n)$. $\frac{d}{dt} = \frac{\partial}{\partial t} + \frac{\partial x}{\partial t}\frac{\partial}{\partial x}$ denotes the material derivatives along characteristics. The order of approximation we mentioned in this subsection is for temporal accuracy. We propose to use a spectrally accurate fast Fourier transform (FFT) in solving the Poisson's Eq. (1.2), whose r.h.s. function $\rho(x,t) = \int f(x,v,t)dv$ is evaluated by a mid-point rule numerically. The mid point rule is of spectral accuracy given the function being integrated is either periodic or compactly supported [4].

2.2.1 First Order Scheme

We let

$$x_i^{n,(1)} = x_i - v_j \Delta t; \quad v_j^{n,(1)} = v_j - E_i^n \Delta t, \tag{2.3}$$

which are first order approximations to $x_i^\star$ and $v_j^\star$, see Proposition 2.1 below. Let

$$f_{i,j}^{n+1,(1)} = f(x_i^{n,(1)}, v_j^{n,(1)}, t^n), \tag{2.4}$$

which is a first order in time approximation to the exact solution $f(x_i, v_j, t^{n+1})$. Note that the spatial approximation in Eq. (2.4) (and in other similar equations in this subsection) is performed via high order WENO interpolation discussed in Sect. 2.3. Based on $\{f_{i,j}^{n+1,(1)}\}$, we compute

$$\rho_i^{n+1,(1)}, \quad E_i^{n+1,(1)}$$

by using a mid-point rule and FFT based on the Poisson's Eq. (1.2). Note that $\rho_i^{n+1,(1)}$ and $E_i^{n+1,(1)}$ also approximate $\rho(x_i, t^{n+1})$ and $E(x_i, t^{n+1})$ with first order temporal accuracy.

Proposition 2.1 *$x_i^{n,(1)}$ and $v_j^{n,(1)}$ constructed in Eq. (2.3) are first order approximations to $x_i^\star$ and $v_j^\star$ in time.*

Proof By Taylor expansion,

$$\begin{aligned} x_i^\star &= x_i - \frac{dx_i}{dt}(x_i, v_j, t^{n+1})\Delta t + \mathcal{O}(\Delta t^2) \\ &= x_i - v_j \Delta t + \mathcal{O}(\Delta t^2) \\ &\overset{(2.3)}{=} x_i^{n,(1)} + \mathcal{O}(\Delta t^2), \\ v_j^\star &= v_j - \frac{dv_j}{dt}|_{t^{n+1}} \Delta t + \mathcal{O}(\Delta t^2) \\ &= v_j - E_i^{n+1} \Delta t + \mathcal{O}(\Delta t^2) \\ &= v_j - (E_i^n + \mathcal{O}(\Delta t))\Delta t + \mathcal{O}(\Delta t^2) \\ &\overset{(2.3)}{=} v_j^{n,(1)} + \mathcal{O}(\Delta t^2). \end{aligned}$$

Hence $x_i^{n,(1)}$ and $v_j^{n,(1)}$ are second order approximations to $x_i^\star$ and $v_j^\star$ locally in time for a time step; the approximation is of first order in time globally. We remark that the proposed first order scheme is similar to, but different from, the standard forward Euler or backward Euler integrator. It is specially tailored to the system (2.1). □

2.2.2 Second Order Scheme

We let

$$x_i^{n,(2)} = x_i - \frac{1}{2}(v_j + v_j^{n,(1)})\Delta t, \quad v_j^{n,(2)} = v_j - \frac{1}{2}(E(x_i^{n,(1)}, t^n) + E_i^{n+1,(1)})\Delta t, \quad (2.5)$$

which are second order approximations to $x_i^\star$ and $v_j^\star$, see Proposition 2.2 below. Note that $E(x_i^{n,(1)}, t^n)$ in Eq. (2.5) can be approximated by WENO interpolation from $\{E_i^n\}_{i=1}^{n_x}$. Let $f_{i,j}^{n+1,(2)} = f(x_i^{n,(2)}, v_j^{n,(2)}, t^n)$, approximating $f(x_i, v_j, t^{n+1})$ with second order in time. Based on $\{f_{i,j}^{n+1,(2)}\}$, we compute $\rho_i^{n+1,(2)}$, $E_i^{n+1,(2)}$ approximating $\rho(x_i, t^{n+1})$ and $E(x_i, t^{n+1})$ with second order temporal accuracy.

Proposition 2.2 *$x_i^{n,(2)}$ and $v_j^{n,(2)}$ constructed in Eq. (2.5) are second order approximations to $x_i^\star$ and $v_j^\star$ in time.*

Proof It can be checked by Taylor expansion

$$\begin{aligned} x_i^\star &= x_i - \left(\frac{dx}{dt}(x_i, v_j, t^{n+1}) + \frac{dx}{dt}(x_i^\star, v_j^\star, t^n)\right)\frac{\Delta t}{2} + \mathcal{O}(\Delta t^3) \\ &= x_i - \left(v_j^\star + v_j\right)\frac{\Delta t}{2} + \mathcal{O}(\Delta t^3) \\ &\overset{Prop.\ 2.1}{=} x_i - \left(v_j^{n,(1)} + \mathcal{O}(\Delta t^2) + v_j\right)\frac{\Delta t}{2} + \mathcal{O}(\Delta t^3) \\ &= x_i - \left(v_j^{n,(1)} + v_j\right)\frac{\Delta t}{2} + \mathcal{O}(\Delta t^3) \\ &\overset{(2.5)}{=} x_i^{n,(2)} + \mathcal{O}(\Delta t^3). \end{aligned}$$

Similarly,

$$\begin{aligned} v_j^\star &= v_j - \left(E_i^{n+1} + E(x_i^\star, t^n)\right)\frac{\Delta t}{2} + \mathcal{O}(\Delta t^3) \\ &\overset{Prop.\ 2.1}{=} v_j - \left(E_i^{n+1,(1)} + E(x_i^{n,(1)}, t^n) + \mathcal{O}(\Delta t^2)\right)\frac{\Delta t}{2} + \mathcal{O}(\Delta t^3) \\ &\overset{(2.5)}{=} v_j^{n,(2)} + \mathcal{O}(\Delta t^3). \end{aligned}$$

Hence $x_i^{n,(2)}$ and $v_j^{n,(2)}$ are third order approximations to $x_i^\star$ and $v_j^\star$ locally in time for a time step; the approximation is of second order in time globally. Again the proposed second order scheme tailored to the system (2.1) is similar to, but slightly different from, the second order Runge–Kutta integrator based on the trapezoid rule. □

2.2.3 Third Order Scheme

We let

$$x_i^{n,(3)} = x_i - v_j\Delta t + \frac{\Delta t^2}{2}\left(\frac{2}{3}E_i^{n+1,(2)} + \frac{1}{3}E(x_i^{n,(2)}, t^n)\right), \tag{2.6}$$

$$v_j^{n,(3)} = v_j - E_i^{n+1,(2)}\Delta t + \frac{\Delta t^2}{2}\left(\frac{2}{3}\left(\frac{d}{dt}E(x_i, t^{n+1})\right)^{(2)} + \frac{1}{3}\frac{d}{dt}E(x_i^{n,(2)}, t^n)\right), \tag{2.7}$$

which are third order approximations to $x_i^\star$ and $v_j^\star$, see Proposition 2.4 below. Note that $\frac{d}{dt}E$ terms on the r.h.s. of Eq. (2.7) will be obtained by using the macro-equations described below. Let $f_{i,j}^{n+1,(3)} = f(x_i^{n,(3)}, v_j^{n,(3)}, t^n)$, approximating $f(x_i, v_j, t^{n+1})$ with third order in time. Based on $\{f_{i,j}^{n+1,(3)}\}$, we compute $\rho_i^{n+1,(3)}$, $E_i^{n+1,(3)}$ approximating $\rho(x_i, t^{n+1})$ and $E(x_i, t^{n+1})$ with third order temporal accuracy.

Remark 2.3 We note that the mechanism to build this third order scheme is different from Runge–Kutta methods where intermediate stage solutions are constructed. It has some similarity in spirit to the Lax–Wendroff type method, where higher order time derivatives are recursively transformed into spatial derivatives. The difference with the Lax–Wendroff type time integration is: Lax–Wendroff method only uses spatial derivatives at one time level, while the proposed method uses the spatial derivatives (or its high order approximations) at both t^n and t^{n+1} via a predictor–corrector procedure. In a sense, the proposed method is a two-stage multi-derivative method.

With $\frac{\partial E}{\partial x} = \rho - 1$ from the Poisson's Eq. (1.2), to compute the Lagrangian time derivative along characteristics $\frac{d}{dt}E = \frac{\partial E}{\partial t} + v\frac{\partial E}{\partial x}$, we only need to numerically approximate $\frac{\partial E}{\partial t}$. Notice that if we integrate the Vlasov Eq. (1.1) over v, we have

$$\rho_t + J_x = 0, \tag{2.8}$$

where $\rho(x,t)$ is the charge density and $J(x,t) = \int f v dv$ is the current density. With the Poisson's Eq. (1.2), and from Eq. (2.8), we have $\frac{\partial}{\partial x}(E_t + J) = 0$, that is $E_t + J$ is independent of the spatial variable x. Thus

$$E_t + J = \frac{1}{L}\int (E_t + J(x,t))dx = \frac{1}{L}\int J(x,t)dx,$$

the last equality above is due to the periodic boundary condition on the potential. It can be shown, by multiplying the Vlasov Eq. (1.1) by v and performing integration in both x- and v- directions, that

$$\frac{\partial}{\partial t}\int J(x,t)dx = 0,$$

therefore

$$\frac{\partial}{\partial t}E(x,t) + J = \frac{1}{L}\int j(x,t=0)dx \doteq \bar{J}^0,$$

where $\bar{\cdot}$ denotes one's spatial average. Hence,

$$\frac{d}{dt}E = \left(\frac{\partial}{\partial t} + v\frac{\partial}{\partial x}\right)E = \bar{J}^0 - J(x,t) + v(\rho - 1). \tag{2.9}$$

Specifically, in Eq. (2.7)

$$\left(\frac{d}{dt}E(x_i,t^{n+1})\right)^{(2)} = \bar{J}^0 - J_i^{n+1,(2)} + v_j(\rho_i^{n+1,(2)} - 1),$$
$$\frac{d}{dt}E(x_i^{n,(2)},t^n) = \bar{J}^0 - J(x_i^{n,(2)},t^n) + v_j^{n,(2)}(\rho(x_i^{n,(2)},t^n) - 1).$$

Note that $J_i^{n+1,(2)}$ and J_i^n can be evaluated by mid-point rule from $\{f_{i,j}^{n+1,(2)}\}$ and $\{f_{i,j}^n\}$ respectively with spectral accuracy in space; while $J(x_i^{n,(2)},t^n)$ can be numerically approximated by WENO interpolation from J_i^n.

Proposition 2.4 *$x_i^{n,(3)}$ and $v_j^{n,(3)}$ constructed in Eqs. (2.6)–(2.7) are third order approximations to $x_i^\star$ and $v_j^\star$ in time.*

Proof It can be checked by Taylor expansion

$$\begin{aligned}
x_i^\star &= x_i - \frac{dx}{dt}(x_i,v_j,t^{n+1})\Delta t + \left(\frac{2}{3}\frac{d^2x_i}{dt^2}(x_i,v_j,t^{n+1}) + \frac{1}{3}\frac{d^2x_i}{dt^2}(x_i^\star,v_j^\star,t^n)\right)\frac{\Delta t^2}{2}\\
&\quad +\mathcal{O}(\Delta t^4)\\
&= x_i - v_j\Delta t + \left(\frac{2}{3}E_i^{n+1} + \frac{1}{3}E(x_i^\star,t^n)\right)\frac{\Delta t^2}{2} + \mathcal{O}(\Delta t^4)\\
&\overset{Prop.\ 2.2}{=} x_i - v_j\Delta t + \left(\frac{2}{3}E_i^{n+1,(2)} + \frac{1}{3}E(x_i^{n,(2)},t^n) + \mathcal{O}(\Delta t^3)\right)\frac{\Delta t^2}{2} + \mathcal{O}(\Delta t^4)\\
&\overset{(2.5)}{=} x_i^{n,(3)} + \mathcal{O}(\Delta t^4).
\end{aligned}$$

Similarly,

$$\begin{aligned}
v_j^\star &= v_j - E_i^{n+1}\Delta t + \left(\frac{2}{3}\frac{dE}{dt}(x_i,t^{n+1}) + \frac{1}{3}\frac{dE}{dt}(x_i^\star,t^n)\right)\frac{\Delta t^2}{2} + \mathcal{O}(\Delta t^4)\\
&\overset{Prop.\ 2.2}{=} v_j - (E_i^{n+1,(2)} + \mathcal{O}(\Delta t^3))\Delta t\\
&\quad +\left(\frac{2}{3}\left(\frac{dE}{dt}(x_i,t^{n+1})\right)^{(2)} + \frac{1}{3}\frac{dE}{dt}(x_i^{n,(2)},t^n) + \mathcal{O}(\Delta t^3)\right)\frac{\Delta t^2}{2} + \mathcal{O}(\Delta t^4)\\
&\overset{(2.5)}{=} v_j^{n,(3)} + \mathcal{O}(\Delta t^4).
\end{aligned}$$

Hence $x_i^{n,(3)}$ and $v_j^{n,(3)}$ are fourth order approximations to $x_i^\star$ and $v_j^\star$ locally in time for a time step; the approximation is of third order in time globally. □

2.2.4 Higher Order Extensions

The procedures proposed above for locating the foot of characteristics can be extended to schemes with higher order temporal accuracy by using higher order version of Taylor expansion, e.g. as in Eqs. (2.6) and (2.7). As higher order material derivatives, e.g. $\frac{d^2}{dt^2}E$, are involved, a set of macro-equations from the Vlasov equation are needed. Specifically, we propose to multiply the Vlasov Eq. (1.1) by v^k, integrate over v and obtain

$$\frac{\partial}{\partial t}M_k + \frac{\partial}{\partial x}M_{k+1} - kEM_{k-1} = 0,$$

where $M_k(x,t) = \int f(x,v,t)v^k dv$. Especially, $M_0 = \rho(x,t)$ is the charge density and $M_1 = J(x,t)$ is the current density. When $k = 0$, we have Eq. (2.8); When $k = 1$, we have

$$\frac{\partial}{\partial t}J + \frac{\partial}{\partial x}M_2 - E\rho = 0. \tag{2.10}$$

With these, we have

$$\begin{aligned}\frac{d^2E}{dt^2} &\overset{(2.9)}{=} \left(\frac{\partial}{\partial t} + v\frac{\partial}{\partial x}\right)(\bar{J^0} - J(x,t) + v(\rho - 1)) \\ &\overset{(2.10)}{=} v^2\frac{\partial \rho}{\partial x} + \frac{\partial M_2}{\partial x} - 2v\frac{\partial J}{\partial x} - E,\end{aligned} \tag{2.11}$$

where spatial derivative terms can be evaluated by high order WENO interpolations or reconstructions.

2.3 High Order WENO Interpolations

In this subsection, we discuss the procedures in spatial interpolation to recover information among grid points to update numerical solution by Eq. (2.2), and in spatial reconstruction to recover function derivatives at grid points, e.g. in computing spatial derivatives in Eq. (2.11). There have been a variety of interpolation choices, such as the piecewise parabolic method (PPM) [14], spline interpolation [15], cubic interpolation propagation (CIP) [36], ENO/WENO interpolation [5,31]. In our work we adapt the WENO interpolations.

2.3.1 WENO Interpolations

High order accuracy is achieved by using several points in the neighborhood: the number of points used in the interpolation determines the order of interpolation. WENO [5,13,31], short for 'weighted essentially non-oscillatory', is a well-developed adaptive procedure to overcome Gibbs phenomenon, when the solution is under-resolved or contains discontinuity. Specifically, when the solution is smooth the WENO interpolation recovers the linear interpolation for very high order accuracy; when the solution is under-resolved, the WENO interpolation automatically assigns more weights to smoother stencils. The smoothness of the stencil is measured by the divided differences of numerical solutions. Below we provide formulas for the sixth order WENO interpolation, which is what we used in our simulations. The reason we choose to use such high order WENO interpolation is that we would like to

make the temporal error the dominant one in our numerical studies, since the focus of current paper is on temporal discretization of characteristics.

The sixth order WENO interpolation at a position $x \in [x_{i-1}, x_i]$ (or $\xi \doteq \frac{x-x_i}{\Delta x} \in [-1, 0]$) is obtained by

$$Q(\xi) = \omega_1 P_1(\xi) + \omega_2 P_2(\xi) + \omega_3 P_3(\xi),$$

where

$$P_1(\xi) = (f_{i-3}, f_{i-2}, f_{i-1}, f_i) \begin{pmatrix} 0 & -1/3 & -1/2 & -1/6 \\ 0 & 3/2 & 2 & 1/2 \\ 0 & -3 & -5/2 & -1/2 \\ 1 & 11/6 & 1 & 1/6 \end{pmatrix} \begin{pmatrix} 1 \\ \xi \\ \xi^2 \\ \xi^3 \end{pmatrix},$$

$$P_2(\xi) = (f_{i-2}, f_{i-1}, f_i, f_{i+1}) \begin{pmatrix} 0 & 1/6 & 0 & -1/6 \\ 0 & -1 & 1/2 & 1/2 \\ 1 & 1/2 & -1 & -1/2 \\ 0 & 1/3 & 1/2 & 1/6 \end{pmatrix} \begin{pmatrix} 1 \\ \xi \\ \xi^2 \\ \xi^3 \end{pmatrix},$$

$$P_3(\xi) = (f_{i-1}, f_i, f_{i+1}, f_{i+2}) \begin{pmatrix} 0 & -1/3 & 1/2 & -1/6 \\ 1 & -1/2 & -1 & 1/2 \\ 0 & 1 & 1/2 & -1/2 \\ 0 & -1/6 & 0 & 1/6 \end{pmatrix} \begin{pmatrix} 1 \\ \xi \\ \xi^2 \\ \xi^3 \end{pmatrix}.$$

Linear weights are

$$\gamma_1(\xi) = \frac{1}{20}(\xi - 1)(\xi - 2), \quad \gamma_2(\xi) = -\frac{1}{10}(\xi + 3)(\xi - 2), \quad \gamma_3(\xi) = \frac{1}{20}(\xi + 3)(\xi + 2).$$

Nonlinear weights are chosen to be

$$\omega_m = \frac{\tilde{\omega}_m}{\sum_{l=1}^{3} \tilde{\omega}_l}, \qquad \text{with} \quad \tilde{\omega}_l = \frac{\gamma_l}{(\varepsilon + \beta_l)^2}, \quad l = 1, 2, 3,$$

where $\epsilon = 10^{-6}$, and the smoothness indicators are

$$\begin{aligned} \beta_1 &= -9\, f_{i-3} f_{i-2} + 4/3\, {f_{i-3}}^2 - 11/3\, f_{i-3} f_i + 10\, f_{i-3} f_{i-1} + 14\, f_{i-2} f_i \\ &\quad + 22\, {f_{i-1}}^2 - 17\, f_{i-1} f_i + 10/3\, {f_i}^2 + 16\, {f_{i-2}}^2 - 37\, f_{i-2} f_{i-1}, \\ \beta_2 &= -7\, f_{i-2} f_{i-1} + 4/3\, {f_{i-2}}^2 - 5/3\, f_{i-2} f_{i+1} + 6\, f_{i-2} U_i + 6\, f_{i-1} f_{i+1} \\ &\quad + 10\, {f_i}^2 - 7\, f_i f_{i+1} + 4/3\, {f_4}^2 + 10\, {f_{i-1}}^2 - 19\, f_{i-1} f_i, \\ \beta_3 &= -17\, f_{i-1} f_i + 10/3\, {f_{i-1}}^2 - 11/3\, f_{i-1} f_{i+2} + 14\, f_{i-1} f_{i+1} + 10\, f_i f_{i+2} \\ &\quad + 16\, {f_{i+1}}^2 - 9\, f_{i+1} f_{i+2} + 4/3\, {f_{i+2}}^2 + 22\, {f_i}^2 - 37\, f_i f_{i+1}. \end{aligned}$$

The above proposed sixth order WENO interpolation has a local truncation error on the order of $\mathcal{O}(\Delta x^6)$ per time step. If such error is considered in local truncation error estimate, see Proposition 2.4, then we would have the following Proposition taking into account the spatial discretization error. Such estimate is being numerically confirmed in the error Table 1 presented in Sect. 3.

Proposition 2.5 *Consider $x_i^{n,(3)}$ and $v_j^{n,(3)}$ constructed in Eqs. (2.6)–(2.7) with the sixth order WENO interpolation as described above. Assume that the local truncation error for the sixth order WENO interpolation for a smooth problem is $\mathcal{O}(\Delta x^6)$, then $x_i^{n,(3)}$ and $v_j^{n,(3)}$ are third order approximations to $x_i^\star$ and $v_j^\star$ in time and fifth order approximations in space.*

Proof Following similar analysis as in Proposition 2.4 but taking into account the error from spatial discretization, we would have

$$x_i^\star = x_i^{n,(3)} + \mathcal{O}(\Delta t^4, \Delta x^6), \tag{2.12}$$

$$v_j^\star = v_j^{n,(3)} + \mathcal{O}(\Delta t^4, \Delta x^6). \tag{2.13}$$

That is $x_i^{n,(3)}$ and $v_j^{n,(3)}$ are fourth order approximations to $x_i^\star$ and $v_j^\star$ in time and sixth order approximations in space *locally for a time step*; the approximation is of third order in time and of order $\mathcal{O}(\Delta x^6/\Delta t)$ in space globally. If one assume $\Delta t = \mathcal{O}(\Delta x)$, the scheme becomes fifth order in space globally. □

Remark 2.6 The main novelty of the proposed method, compared with other existing methods, is the high order way of tracing characteristics in time. We don't foresee any difficulty in extending such high order characteristics tracing algorithm to unstructured mesh, as long as the spatial derivatives can be approximated on the corresponding meshes with proper accuracy and efficiency. Note that this can be achieved in the finite difference setting on a regular Cartesian mesh, which is the case that we consider in this paper. High order WENO reconstruction on unstructured meshes are possible. For example, in the context of finite volume schemes, we mention the work by Dumbser et al. [17] and Liu and Zhang [29].

2.4 Computational Cost and Savings

One of the procedures in the proposed method that takes up much computational time is to trace the foot of characteristics. Assume $N = n_x = n_v$, the scheme involves solving the Poisson's equation via FFT with the cost on the order of $N \log(N)$ and a high order 2-D WENO interpolation on the order of CN^2, where the constant C is larger when the order of interpolation is higher. Since the 2-D WENO interpolation (compared with the 1-D Poisson solver) is a procedure that takes most of the computational time, we will use the number of 2-D WENO interpolations as a measurement of computational cost.

For the first order scheme (2.3), there is a high order 2-D WENO interpolation involved. The proposed second order scheme (2.5) is based on the first order prediction: two high order 2-D WENO interpolations are involved. This leads to twice the computational cost as the first order scheme. The third order scheme (2.6)–(2.7) is based on the second order prediction: three high order 2-D WENO interpolations are involved. We claim that proposed high order procedures are computationally efficient: the computational cost roughly grows linearly with the order of approximation. To further save some computational cost, we propose to use lower order 2-D WENO interpolation in the prediction steps. Specifically, in the third order scheme (2.6)–(2.7), we propose to use a second order 2-D WENO interpolation in the first order prediction, use a fourth order 2-D WENO interpolation in the second order prediction, and use a sixth order 2-D WENO interpolation in the final step of updating.

3 Numerical Tests: The Vlasov–Poisson System

In this section, we examine the performance of the proposed fully multi-dimensional semi-Lagrangian method for the VP systems. Periodic boundary condition is imposed in x-direction, while zero boundary condition is imposed in v-direction. We recall several quantities in the VP system below, which should remain constant in time.

1. Mass:
$$\text{Mass} = \int_v \int_x f(x, v, t) dx dv.$$
2. L^p norm $1 \leq p < \infty$:
$$\|f\|_p = \left(\int_v \int_x |f(x, v, t)|^p dx dv \right)^{\frac{1}{p}}. \tag{3.14}$$
3. Energy:
$$\text{Energy} = \int_v \int_x f(x, v, t) v^2 dx dv + \int_x E^2(x, t) dx, \tag{3.15}$$
where $E(x, t)$ is the electric field.
4. Entropy:
$$\text{Entropy} = \int_v \int_x f(x, v, t) \log(f(x, v, t)) dx dv. \tag{3.16}$$

Tracking relative deviations of these quantities numerically will be a good measure of the quality of numerical schemes. The relative deviation is defined to be the deviation away from the corresponding initial value divided by the magnitude of the initial value. In our numerical tests, we let the time step size $\Delta t = CFL \cdot \min(\Delta x / v_{max}, \Delta v / \max(E))$, where CFL is specified for different runs; and let $v_{max} = 6$ to minimize the error from truncating the domain in v-direction.

We first present the example of two stream instability, for which we will demonstrate the (1) high order spatial accuracy and the high order temporal accuracy of the proposed schemes; (2) the time evolution of overall mass and other theoretically conserved physical norms for the proposed method; (3) the performance of the proposed method in resolving solution structures.

Example 3.1 Consider two stream instability [19], with an unstable initial distribution function:
$$f(x, v, t = 0) = \frac{2}{7\sqrt{2\pi}} (1 + 5v^2)(1 + \alpha((\cos(2kx) + \cos(3kx))/1.2 + \cos(kx)) \exp\left(-\frac{v^2}{2}\right) \tag{3.17}$$
with $\alpha = 0.01$, $k = 0.5$, the length of the domain in the x direction is $L = \frac{2\pi}{k}$ and the background ion distribution function is fixed, uniform and chosen so that the total net charge density for the system is zero.

We test both spatial and temporal convergence of the proposed truly multi-dimensional semi-Lagrangian method. We first test the spatial convergence by using a sequence of meshes with $n_x = n_v = \{210, 126, 90, 70\}$. The meshes are designed so that the coarse mesh grid coincides with part of the reference fine mesh grid ($n_x = n_v = 630$). The errors are measured by comparing the numerical solution with that on the reference fine grid with 630×630 grid points. We set $CFL = 0.01$ so that the spatial error is the dominant error. Table 1 is the spatial convergence table for the proposed schemes with sixth order WENO interpolation. The expected fifth order convergence globally in time in observed. An alternative way of checking the convergence of the proposed scheme is to make use of the time reversibility of the VP system. In particular, one can firstly integrate the system forward to some time T, and then reverse the process and integrate the system backward by the same amount of time T. After such forward and backward integration processes, the system should recover

Table 1 Two stream instability: test order of accuracy in space for the SL WENO schemes by comparing numerical solutions with a reference solution from a simulation with a set of refined mesh

$n_x \times n_v$	L^1 error	Order
70×70	7.01E-7	–
90×90	2.06E-7	4.88
126×126	3.96E-8	4.89
210×210	3.20E-9	4.95

The scheme use sixth order WENO interpolation and has a third order temporal accuracy in tracing characteristics. $T = 1$ and $CFL = 0.01$. We set $CFL = 0.01$ so that the spatial error is the dominant error

Table 2 Two stream instability: test order of accuracy in space for the SL WENO schemes via the time reversibility of the system

$n_x \times n_v$	L^1 error	Order
60×60	1.52E-6	–
80×80	4.17E-7	4.53
100×100	1.43E-7	4.78
120×120	6.00E-8	4.76
140×140	2.90E-8	4.82

The scheme use sixth order WENO interpolation and has a third order temporal accuracy in tracing characteristics. $T = 0.5$ and $CFL = 0.01$. We set $CFL = 0.01$ so that the spatial error is the dominant error

the initial condition, which can be used as a reference solution. We show errors and the corresponding orders in Table 2 by the above-mentioned time reversibility property for testing spatial convergence. We then test the temporal convergence of the proposed first, second and third order schemes. Table 3 provides the temporal convergence rate for the scheme with the first to third order temporal accuracy. We use the sixth order WENO interpolation and a spatial mesh of $n_x = n_v = 160$, so that the temporal error is the dominant error. The reference solution is computed by using the same spatial mesh but with relatively small $CFL = 0.1$. In Table 3, the time step size is about 6 to 10 times that from an Eulerian method, yet highly accurate numerical results is achieved. Expected first, second and third order temporal accuracy are observed. On the rightmost column of Table 3, we show errors and the corresponding orders of convergence with CFL ranging from 1 to 5. One can see that the spatial error starts to dominate as CFL decreases, thus the theoretical order of convergence in time can no longer be observed.

To compare the performance of schemes with different temporal orders, we numerically track the time evolution of physically conserved quantities of the system. In our runs, we let $n_x = n_v = 128$, $CFL = 5$. In Fig. 1, the time evolution of numerical L^1 norm, L^2 norm, energy and entropy for schemes with different orders of temporal accuracy are plot. In general, high order temporal accuracy indicates a better preservation of those physically conserved norms. The L^1 norm is not conserved since our scheme is neither mass conservative nor positivity preserving. We also check the mass conservation over time $\int_v \int_x f(x, v, t)dxdv$, which is the same as the L^1 norm if f is positive. For this example, the time evolution of mass and L^1 norm appear to be the same, indicating positivity of the solution. In Fig. 2, we show the contour plot and slices of the numerical solution of the proposed SL WENO

Table 3 Two stream instability. $n_x = n_v = 160$ and $T = 5$

CFL	First order		Second order		Third order		CFL	Third order	
	L^1 error	Order	L^1 error	Order	L^1 error	Order	CFL	L^1 error	Order
6	1.17E-4	–	2.40E-6	–	1.13E-7	3.00	1	1.70E-9	–
7	1.40E-4	1.13	2.80E-6	2.04	1.79E-7	3.02	2	5.00E-9	1.60
8	1.63E-4	1.16	3.69E-6	2.07	2.69E-7	3.02	3	1.44E-8	2.60
9	1.87E-4	1.16	4.69E-6	2.04	3.84E-7	3.03	4	3.35E-8	2.93
10	2.12E-4	1.20	5.84E-6	2.08	5.31E-7	3.065	5	6.52E-8	2.97

Order of accuracy in time for the SL WENO schemes with sixth order WENO interpolation and various orders of temporal accuracy. The rightmost column is for the third order scheme with CFL ranging from 1 to 5. One can see that the spatial error starts to dominate as CFL decreases, thus the theoretical order of convergence in time can no longer be observed

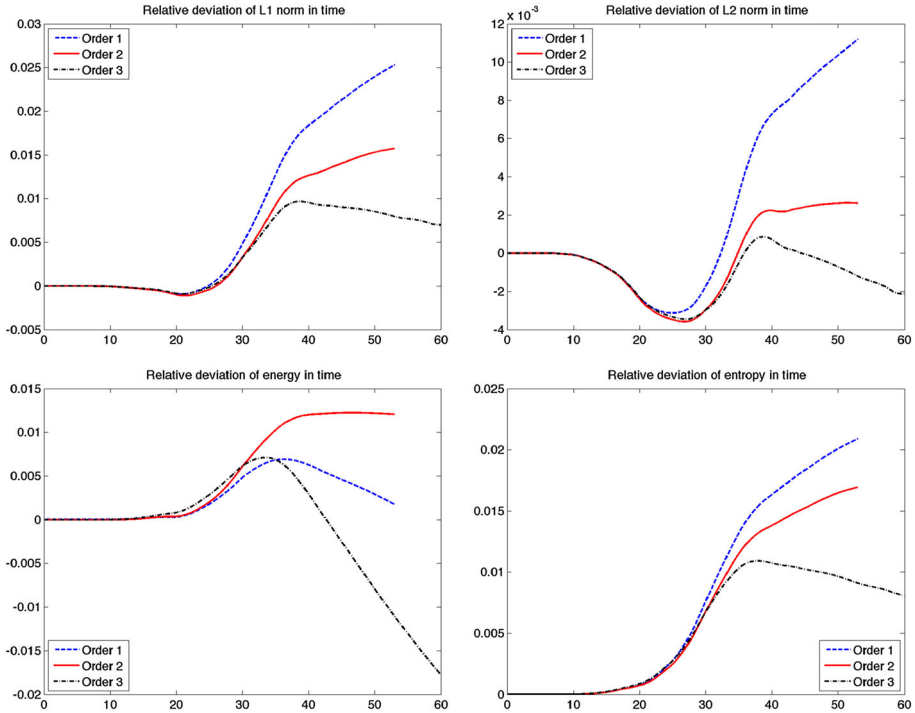

Fig. 1 Two stream instability. The SL WENO scheme with sixth order WENO interpolation in space and various orders of temporal accuracy. Time evolution of the relative deviations of discrete L^1 norms (*upper left*), L^2 norms, kinetic energy norms (*lower left*) and entropy (*lower right*)

method with third order temporal accuracy at $T = 60$. The plot is comparable to our earlier work reported in [30,31].

Example 3.2 Consider weak Landau damping for the Vlasov–Poisson system with initial condition:

$$f(x, v, t = 0) = \frac{1}{\sqrt{2\pi}}(1 + \alpha \cos(kx)) \exp\left(-\frac{v^2}{2}\right), \tag{3.18}$$

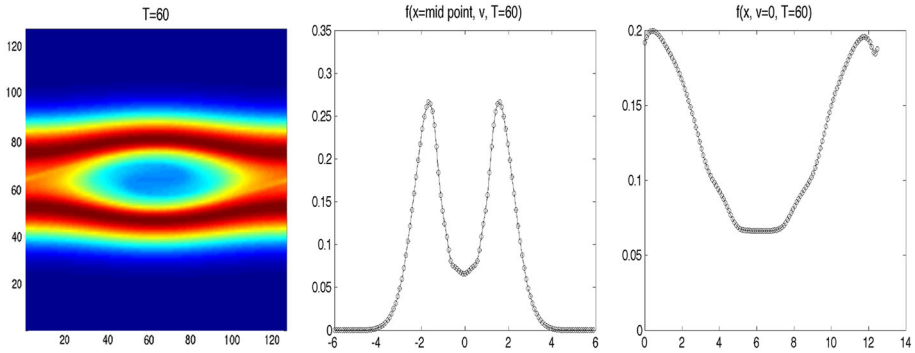

Fig. 2 Two stream instability: $T = 60$. The SL WENO scheme with the sixth order WENO interpolation and a third order temporal accuracy. The spatial mesh is 128×128 and $CFL = 5$. *Left panel* presents the contour plot of the numerical solution, with middle and *right panels* presenting slices of numerical solutions at mid points of spatial domain and at $v = 0$ respectively

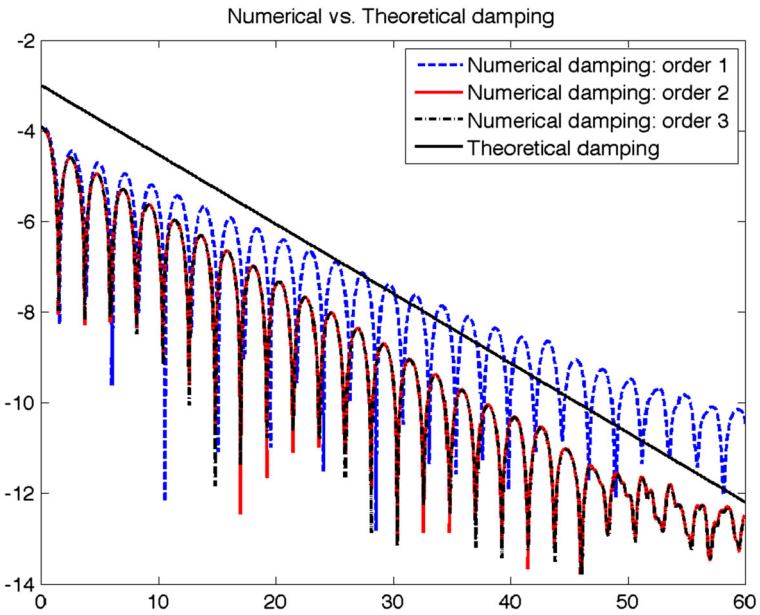

Fig. 3 Weak Landau damping. Time evolution of electric field in L^2 norm

where $\alpha = 0.01$. When the perturbation magnitude is small enough ($\alpha = 0.01$), the VP system can be approximated by linearization around the Maxwellian equilibrium $f^0(v) = \frac{1}{\sqrt{2\pi}} e^{-\frac{v^2}{2}}$. The analytical damping rate of electric field can be derived accordingly [21]. We test the numerical numerical damping rates with theoretical values. We only present the case of $k = 0.5$. The spatial computational grid has $n_x = n_v = 128$ and $CFL = 5$.

For the scheme with first, second and third order accuracy in time and sixth order WENO interpolation in space, we plot the evolution of electric field in L^2 norm benchmarked with theoretical values (solid black lines in the figure) in Fig. 3. A better match with the theoretical decay rate of the electric field is observed for schemes with second and third order temporal

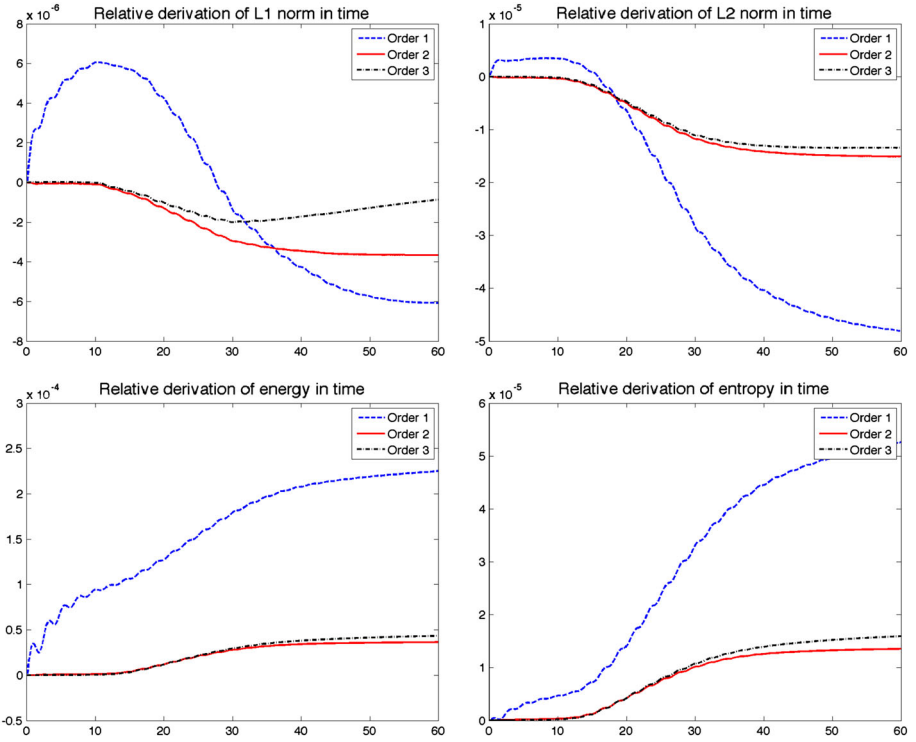

Fig. 4 Weak Landau damping. The proposed SL WENO scheme with first, second and third order accuracy in time and sixth order WENO interpolation in space. Time evolution of the relative deviations of discrete L^1 norms (*upper left*), L^2 norms, kinetic energy norms (*lower left*) and entropy (*lower right*)

accuracy. The time evolution of discrete L^1 norm, L^2 norm, kinetic energy and entropy of schemes with different temporal orders are reported in Fig. 4. L^1 and L^2 norms are better preserved by schemes with higher order temporal accuracy. Note that the mass is not exactly preserved. Energy and entropy are better preserved by schemes with second and third order accuracy than that with first order accuracy. For this weak Landau damping test, the time evolution of the mass exactly coincides with that of the L^1 norm, indicating that there is no negative values in the function f.

Example 3.3 Consider strong Landau damping. The initial condition is Eq. (3.18), with $\alpha = 0.5$ and $k = 0.5$. The evolution of L^2 norms of electric field is provided in Fig. 5, which is comparable to existing results in the literature, e.g. see [24]. The time evolution of discrete mass, L^1 norm, L^2 norm, kinetic energy and entropy are reported in Fig. 6. The L^1 norm, as expected, is not conservative. Numerical solutions of the proposed scheme at different times are observed to be comparable to those that have been well reported in the literature, e.g. [24,30] among many others. Thus we omit to present those figures to save space.

Example 3.4 Consider the symmetric two stream instability [1], with the initial condition

$$f(x, v, t = 0) = \frac{1}{\sqrt{8\pi}\, v_{th}} \left[\exp\left(-\frac{(v-u)^2}{2v_{th}^2} \right) + \exp\left(-\frac{(v+u)^2}{2v_{th}^2} \right) \right] \left(1 + 0.0005 \cos(kx)\right) \tag{3.19}$$

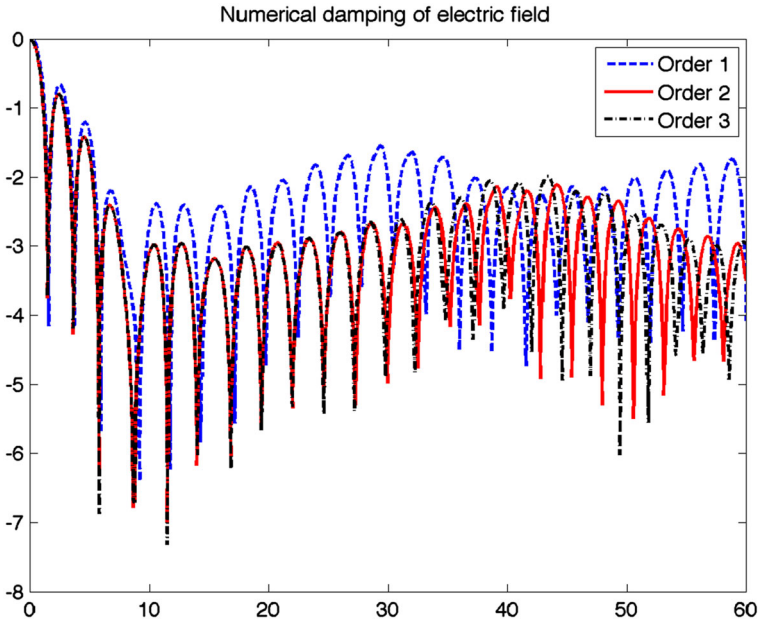

Fig. 5 Strong Landau damping. Time evolution of electric field in L^2 norm

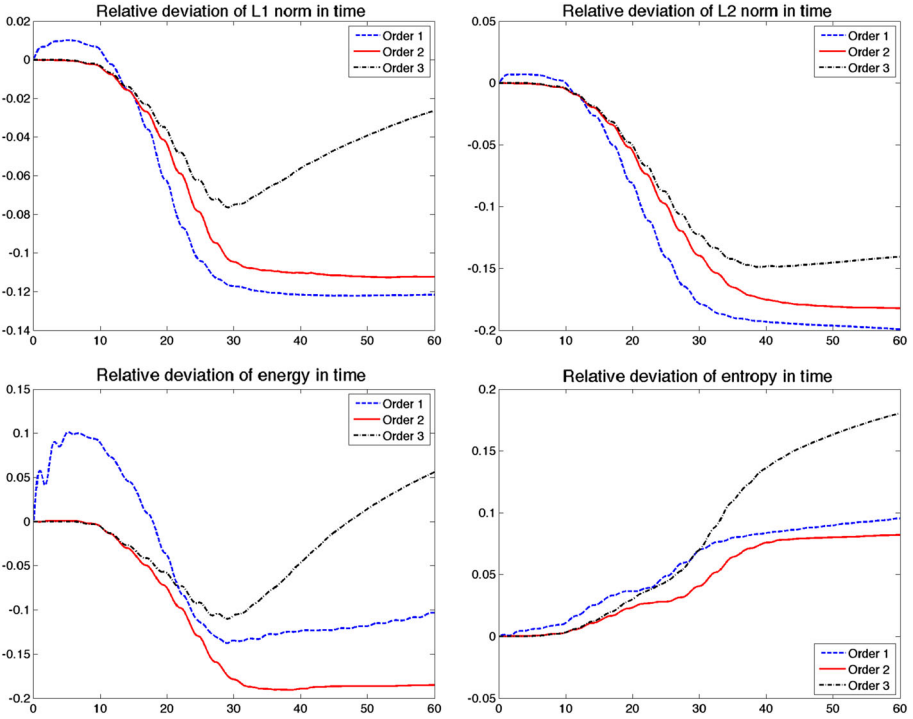

Fig. 6 Strong Landau damping. The SL WENO scheme with sixth order WENO interpolation in space and various orders of temporal accuracy. Time evolution of the relative deviations of discrete L^1 norms (*upper left*), L^2 norms, kinetic energy norms (*lower left*) and entropy (*lower right*)

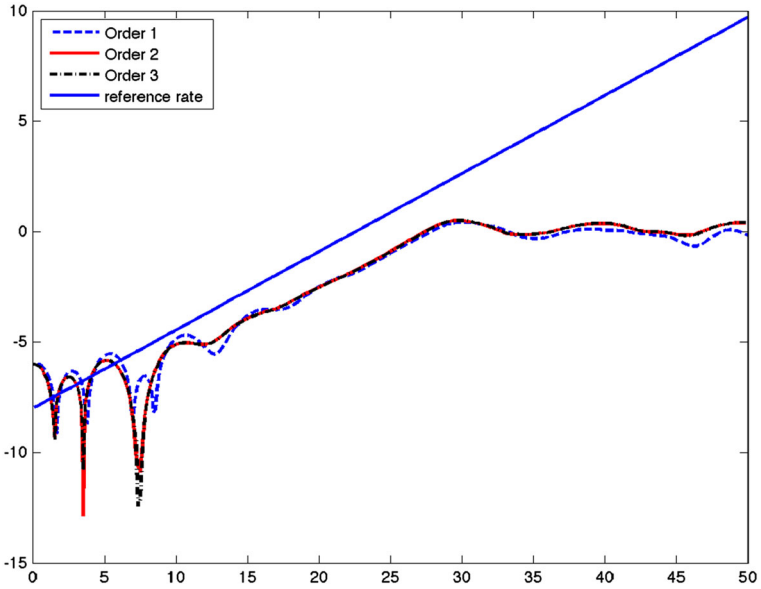

Fig. 7 Symmetric two stream instability: time evolution of electric field in L^2 norm. The SL WENO scheme with sixth order WENO interpolation in space and various orders of temporal accuracy

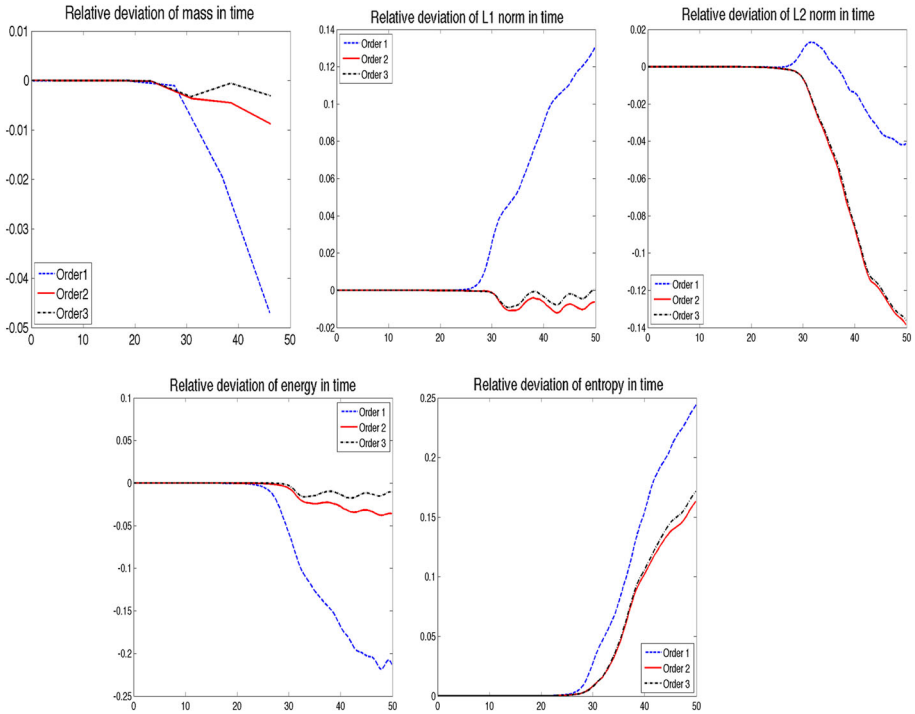

Fig. 8 Symmetric two stream instability. The SL WENO scheme with sixth order WENO interpolation in space and various orders of temporal accuracy. Time evolution of the relative deviations of discrete mass (*upper left*), L^1 norms (*upper middle*), L^2 norms, kinetic energy norms (*lower left*) and entropy (*lower right*)

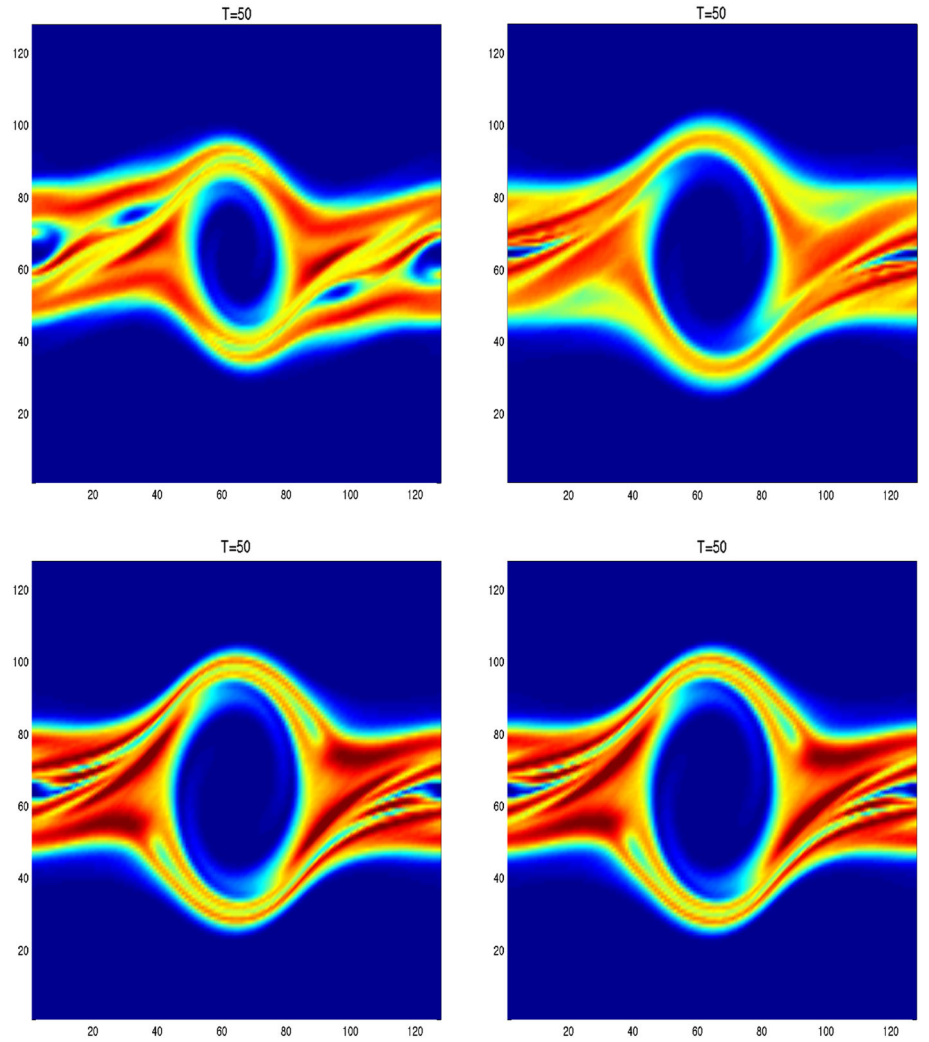

Fig. 9 Symmetric two stream instability: $T = 50$. Results from schemes with first order temporal accuracy with $CFL = 5$ (*upper left*), $CFL = 0.1$ (*upper right*). Results from schemes with second order temporal accuracy (*lower left*) and third order temporal accuracy (*lower right*) and $CFL = 5$

with $u = 5\sqrt{3}/4$, $v_{th} = 0.5$ and $k = 0.2$. The background ion distribution function is fixed, uniform and chosen so that the total net charge density for the system is zero. We use a mesh of 128×128 and $CFL = 5$. Figure 7 plots the evolution of electric fields for the proposed scheme benchmarked with a reference rate from linear theory $\gamma = \frac{1}{\sqrt{8}}$, see [1]. Theoretical consistent results are observed. Time evolution of discrete mass, L^1 norm, L^2 norm, kinetic energy and entropy of schemes with different temporal orders are reported in Fig. 8. Again, higher order schemes in general perform better in preserving the conserved physical quantities than low order ones. The mass conservation over time $\int_v \int_x f(x, v, t)dxdv$ is different from the L^1 norm, since our scheme is not positivity preserving. The first two upper panels in Fig. 8 indicates how much of the mass conservation and positivity are preserved at the discrete level.

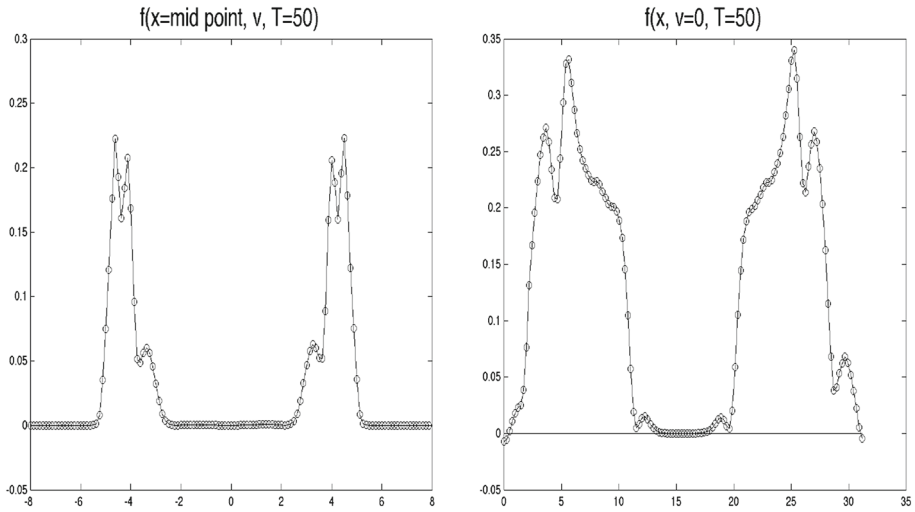

Fig. 10 Symmetric two stream instability. Slices of numerical solutions of the scheme with third order temporal accuracy and $CFL = 5$. *Left*: the solution $f(x, v, T = 50)$ with x located at the mid point of the domain. *Right*: the solution $f(x, v = 0, T = 50)$ with a reference line $y = 0$. It can be observed from the *right panel* that the numerical solution does not strictly preserve positivity

In Fig. 9, we report numerical solutions from the SL WENO schemes with various temporal accuracy in approximating the distribution solution f. It can be observed that, with the same time step size, the higher order schemes (e.g. second and third order ones) perform better than a first order one. For this example, we also show two slides of numerical solutions in Fig. 10. It can be observed that our scheme does not preserve positivity of the solution. The positivity error, however, is small and quickly decreases as the grid is refined. We measure the positivity error, defined as

$$\text{err}_p = \frac{\|f\|_1 - \int_x \int_v f(x, v, t)\, dv\, dx}{\|f\|_1}.$$

For a mesh of 128×128, the positivity error is measured as $8.00E-5$. While we refine the mesh to 256×256, the positivity error is measured as $1.73E-5$, indicating a decay of positivity error with mesh refinement. Designing schemes with mass conservation and positivity is of great importance and this constitutes our ongoing and future work [35].

4 Conclusion

In this paper, we propose a systematic way of tracing characteristics for a one-dimensional in space and one-dimensional in velocity Vlasov–Poisson system with high order temporal accuracy. Based on such mechanism, a finite difference grid-based semi-Lagrangian approach coupled with WENO interpolation is proposed to evolve the system. It is numerically demonstrated that schemes with higher order of temporal accuracy perform better in many aspects than the first order ones. Designing mass conservative semi-Lagrangian schemes, yet not subject to time step constraints, is considered to be challenging and is subject to future research investigations.

References

1. Banks, J., Hittinger, J.: A new class of nonlinear finite-volume methods for Vlasov simulation. IEEE Trans. Plasma Sci. **38**, 2198–2207 (2010)
2. Begue, M., Ghizzo, A., Bertrand, P., Sonnendrucker, E., Coulaud, O.: Two-dimensional semi-Lagrangian Vlasov simulations of laser-plasma interaction in the relativistic regime. J. Plasma Phys. **62**, 367–388 (1999)
3. Besse, N., Sonnendrucker, E.: Semi-Lagrangian schemes for the Vlasov equation on an unstructured mesh of phase space. J. Comput. Phys. **191**, 341–376 (2003)
4. Boyd, J.: Chebyshev and Fourier Spectral Methods. Courier Dover Publications, New York (2001)
5. Carrillo, J.A., Vecil, F.: Nonoscillatory interpolation methods applied to Vlasov-based models. SIAM J. Sci. Comput. **29**, 1179 (2007)
6. Casas, F., Crouseilles, N., Faou, E., Mehrenberger, M.: High-order hamiltonian splitting for Vlasov–Poisson equations. arXiv preprint arXiv:1510.01841, (2015)
7. Charles, F., Després, B., Mehrenberger, M.: Enhanced convergence estimates for semi-Lagrangian schemes application to the Vlasov-Poisson equation. SIAM J. Numer. Anal. **51**, 840–863 (2013)
8. Cheng, C., Knorr, G.: The integration of the Vlasov equation in configuration space. J. Comput. Phys. **22**, 330–351 (1976)
9. Cheng, Y., Christlieb, A.J., Zhong, X.: Energy-conserving discontinuous galerkin methods for the vlasov-ampère system. J. Comput. Phys. **256**, 630–655 (2014)
10. Cheng, Y., Gamba, I.M., Proft, J.: Positivity-preserving discontinuous galerkin schemes for linear Vlasov-Boltzmann transport equations. Math. Comput. **81**, 153 (2011)
11. Christlieb, A., Guo, W., Morton, M.M., Qiu, J.-M.: A high order time splitting method based on integral deferred correction for semi-Lagrangian Vlasov simulations. J. Comput. Phys. **267C**, 7–27 (2014)
12. Christlieb, A.J., Hitchon, W.N.G., Keiter, E.R.: A computational investigation of the effects of varying discharge geometry for an inductively coupled plasma. IEEE Trans. Plasma Sci. **28**, 2214–2231 (2000)
13. Cockburn, B., Johnson, C., Shu, C.-W., Tadmor, E.: Advanced Numerical Approximation of Nonlinear Hyperbolic Equations. Springer, New York (1998)
14. Colella, P., Woodward, P.: The piecewise parabolic method(PPM) for gas-dynamical simulations. J. Comput. Phys. **54**, 174–201 (1984)
15. Crouseilles, N., Latu, G., Sonnendrucker, E.: Hermite spline interpolation on patches for parallelly solving the Vlasov-Poisson equation. Int. J. Appl. Math. Comput. Sci. **17**, 335–349 (2007)
16. Crouseilles, N., Mehrenberger, M., Sonnendrücker, E.: Conservative semi-lagrangian schemes for Vlasov equations. J. Comput. Phys. **229**, 1927–1953 (2010)
17. Dumbser, M., Käser, M., Titarev, V.A., Toro, E.F.: Quadrature-free non-oscillatory finite volume schemes on unstructured meshes for nonlinear hyperbolic systems. J. Comput. Phys. **226**, 204–243 (2007)
18. Feng, J., Hitchon, W.: Self-consistent kinetic simulation of plasmas. Phys. Rev. E **61**, 3160 (2000)
19. Filbet, F., Sonnendrücker, E.: Comparison of Eulerian Vlasov solvers. Comput. Phys. Commun. **150**, 247–266 (2003)
20. Filbet, F., Sonnendrücker, E., Bertrand, P.: Conservative numerical schemes for the Vlasov equation. J. Comput. Phys. **172**, 166–187 (2001)
21. Fried, B., Conte, S.: The Plasma Dispersion Function, vol. 1. Academic Press, New York (1961)
22. Friedman, A., Parker, S., Ray, S., Birdsall, C.: Multi-scale particle-in-cell plasma simulation. J. Comput. Phys. **96**, 54–70 (1991)
23. Güçlü, Y., Christlieb, A.J., Hitchon, W.N.: Arbitrarily high order convected scheme solution of the Vlasov-Poisson system. J. Comput. Phys. **270**, 711–752 (2014)
24. Guo, W., Qiu, J.-M.: Hybrid semi-Lagrangian finite element-finite difference methods for the Vlasov equation. J. Comput. Phys. **234**, 108–132 (2013)
25. Heath, R., Gamba, I.M., Morrison, P.J., Michler, C.: A discontinuous Galerkin method for the Vlasov-Poisson system. J. Comput. Phys. **231**, 1140–1174 (2012)
26. Heikkinen, J., Janhunen, S., Kiviniemi, T., Ogando, F.: Full f gyrokinetic method for particle simulation of tokamak transport. J. Comput. Phys. **227**, 5582–5609 (2008)
27. Huot, F., Ghizzo, A., Bertrand, P., Sonnendrucker, E., Coulaud, O.: Instability of the time splitting scheme for the one-dimensional and relativistic Vlasov-Maxwell system. J. Comput. Phys. **185**, 512–531 (2003)
28. Jacobs, G., Hesthaven, J.: Implicit-explicit time integration of a high-order particle-in-cell method with hyperbolic divergence cleaning. Comput. Phys. Commun. **180**, 1760–1767 (2009)
29. Liu, Y., Zhang, Y.-T.: A robust reconstruction for unstructured weno schemes. J. Sci. Comput. **54**, 603–621 (2013)
30. Qiu, J.-M., Christlieb, A.: A conservative high order semi-Lagrangian WENO method for the Vlasov Equation. J. Comput. Phys. **229**, 1130–1149 (2010)

31. Qiu, J.-M., Shu, C.-W.: Conservative semi-Lagrangian finite difference WENO formulations with applications to the Vlasov equation. Commu. Comput. Phys. **10**, 979–1000 (2011a)
32. Qiu, J.-M., Shu, C.-W.: Positivity preserving semi-Lagrangian discontinuous Galerkin methods for Vlasov simulations. J. Comput. Phys. **230**, 8386–8409 (2011b)
33. Rossmanith, J., Seal, D.: A positivity-preserving high-order semi-Lagrangian discontinuous Galerkin scheme for the Vlasov-Poisson equations. J. Comput. Phys. **230**, 6203–6232 (2011)
34. Sonnendruecker, E., Roche, J., Bertrand, P., Ghizzo, A.: The semi-Lagrangian method for the numerical resolution of the Vlasov equation. J. Comput. Phys. **149**, 201–220 (1999)
35. Xiong, T., Russo, G., Qiu, J.-M.: Conservative multi-dimensional semi-lagrangian finite difference scheme: stability and applications to the kinetic and fluid simulations. arXiv preprint arXiv:1607.07409, (2016)
36. Yabe, T., Xiao, F., Utsumi, T.: The constrained interpolation profile method for multiphase analysis. J. Comput. Phys. **169**, 556–593 (2001)
37. Zhou, T., Guo, Y., Shu, C.-W.: Numerical study on Landau damping. Phys. D **157**, 322–333 (2001)